In-Situ Densification of Combustion Synthesized Coatings

Jan A. Puszynski, Shuxia Miao, Bjarni Stefansson, and Sunil Jagarlamudi
Dept. of Chemistry and Chemical Engineering, South Dakota School of Mines and Technology, Rapid City, SD 57701

Dense intermetallic and ceramic (alumina based) coatings can be formed in situ during simultaneous combustion synthesis and densification in the field of centrifugal forces. Both microstructure and composition of alumina-based coatings formed during alumino-thermal reduction of oxides can be altered by an introduction of additives such as $ZrSiO_4$, SiO_2, Na_2CrO_4, and carbon. The activation energy and frequency factor for the Ni-Al reacting system consisting of equal atomic amounts of Ni and Al powders with an average particle size of 5 μm were measured using a nonisothermal technique, which were equal to 1.05×10^5 J/mol and 1.017×10^8 s^{-1}, respectively. A mathematical model of in-situ densification of a single-phase combustion product (NiAl) in the field of centrifugal forces was developed and explored.

Introduction

A new class of processes with enormous technological flexibility and capability called combustion synthesis or self-propagating high-temperature synthesis (SHS) was developed and successfully applied in the last two decades (Merzhanov, 1981; Munir and Anselmi-Tamburini, 1989; Merzhanov, 1990; Luss, 1990; Varma and Lebrat, 1992). Many exothermic noncatalytic gasless reactions liberate enough heat to be self-sustained after being locally ignited. Over two-hundred ceramic and composite powders have been synthesized using this technique (Merzhanov, 1981; Frankhauser et al., 1985; McCauley, 1990).

The combustion technique might be advantageous over conventional synthesis methods, because of very low energy requirements, simplicity, and versatility of a combustion reactor. In addition, a product formed during combustion usually has a higher purity than starting reactants due to evaporation of volatile impurities (Merzhanov, 1990). The major problem associated with SHS reactions is a relatively high porosity of the products due to a volume change during the reaction. The effects of desorption of moisture and vaporization of volatile impurities and reactants (or products), as well as a generation of large thermal stresses across the reaction zone also contribute to a higher porosity (Frankhauser et al., 1985). It has been shown that densification of combustion synthesized materials can be achieved, almost in any case, if any external force is applied during or immediately after the combustion reaction is completed (Frankhauser et al., 1985). Densification can be accomplished by means of uniaxial, isostatic, or centrifugal forces (DeAngelis and Weiss, 1990; Merzhanov and Yukhvid, 1989; Odawara, 1990; Grebe et al., 1992).

The concept of centrifugal-SHS process was first introduced by Russian scientists (Merzhanov and Yukhvid, 1989). A mixture of refractory oxide(s) and aluminum was placed inside a rotating steel pipe. By means of an external energy source, this mixture was later ignited and due to a large centrifugal acceleration, combustion products, typically iron and alumina, were stratified into two different layers due to the difference in their density. The innermost layer consisted mainly of aluminum oxide when the outermost layer, close to the substrate pipe, consisted of the metal. Later, Japanese researchers used this technique to coat 5-m-long, 1-m dia. steel pipes with alumina. This kind of ceramic lined steel pipe exhibits a high resistance to abrasion and corrosion, and good metallic-ceramic bonding makes this coating more resistant to thermal shocks. However, the major advantage of this technique is a very low cost and simplicity of the coating process. This type of coating might find its application in chemical, metallurgical, mining, and petroleum industries.

It can be concluded from previously reported experimental studies (Merzhanov and Yukhvid, 1989) that a higher centrifugal force and preheating of reactant mixture usually lead to better quality of ceramic coatings. Odawara (1990) reduced the porosity of an alumina coating by adding 5 mol %

SiO_2. Yin and coworkers (1993) have shown that the addition of 5 mol % feldspar into Fe_2O_3-Al mixture also reduces the porosity and improves a smoothness of the internal ceramic surface. The main reason to add additives into the Fe_2O_3-Al reacting system is to lower the melting point of a ceramic component. These modifications usually alter product microstructure, as well as chemical and mechanical properties.

So far, the reported research studies in the area of centrifugal SHS densification are mainly of an experimental character. There have been several articles published on uniaxial densification of combustion synthesized products (Buchatskii and Stolin, 1989; Smolyakov, 1988; Stel'makh et al. (1991a,b). The first attempt to model a simultaneous combustion synthesis and densification in a field of centrifugal forces was made by Puszynski et al. (1995).

The objectives of this article are: (1) experimental studies of *in-situ* formation of single- and multiphase coatings in a field of centrifugal forces; (2) measurements of kinetic parameters in Ni-Al system; and (3) mathematical modeling of nonisothermal centrifugal densification of single-phase (NiAl) system.

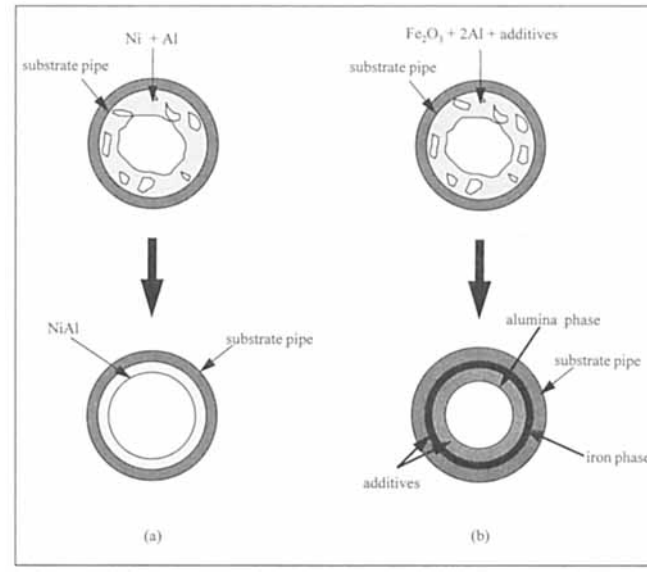

Figure 1. Single- and multiphase SHS centrifugal densification process: (a) Ni-Al system; (b) Fe_2O_3-Al system.

Experimental Studies

In-situ densification of combustion synthesized products

Both single-and multiphase internal coatings of metallic cylindrical substrates were formed using *in-situ* densification of combustion product(s) in a field of centrifugal forces. Source, average particle size, and purity of all reactants and additives listed below is included in parentheses. Aluminum (Reynolds Co., ~ 5 μm, 98.5%); iron oxide, Fe_2O_3 (Solomon Grind-Chem. Service Inc., ~ 1 μm, 99.0%); nickel (INCO Co., ~ 5 μm, 99.0%); chromium oxide, Cr_2O_3 (Solomon Grind-Chem. Service Inc., ~ 1 μm, 99.0%); zircon, $ZrSiO_4$ (TAM Ceramics Inc., ~ 10 μm, 99.0%); silica (Whittaker, Clark & Daniels, Inc., ~ 25 μm, 99.3%); sodium chromate, Na_2CrO_4 (Johnson Mathey Corp., 18 μm, 98.0%); carbon (Colombian Chem. Co., ~ 0.25 μm, 99.5%).

Reactants and additives were dry mixed for 4–6 h in a rotary mixer. Reactant mixture in a form of loose powders was placed inside a rotating cylindrical substrate (carbon steel pipe) and later ignited. Both length and diameter of substrates were varied in these experiments. The reactants were ignited either by uniform preheating of a rotating substrate (Ni-Al system) or by resistively heated molybdenum wire placed at one end of a rotating cylindrical substrate (Fe_2O_3-Al system).

A direct reaction between aluminum and nickel powders was carried in the argon atmosphere to prevent any oxidation of formed nickel aluminide. In order to increase the amount of molten nickel aluminide, the Ni-Al mixture was uniformly heated by an external furnace, while the cylindrical substrate was rotated. Measurements under static conditions (no rotation) had shown that the reaction was spontaneously initiated once the temperature exceeded the eutectic point, 620°C. The temperature of the formed product measured by both an optical pyrometer and W (5% Rh)-W (25% Rh) thermocouples corresponded to the melting point of NiAl phase.

The simultaneous synthesis and densification of nickel aluminide NiAl is shown in Figure 1a. Microstructure of the combustion synthesized NiAl dense product and its X-ray diffraction patterns are shown in Figures 2 and 3, respectively. Pure nickel aluminide phase NiAl was synthesized under these conditions. All peaks in X-ray diffraction pattern correspond to NiAl phase (see Figure 2). When centrifugal acceleration was greater than 150 times the gravitational acceleration, the product with the density greater than 97% of the theoretical one was obtained. In the case of lower centrifugal accelerations ($a < 20 \div 50$ g), the densification process was incomplete and the final product density has not exceeded 70% of the theoretical one.

From the practical and economical point of views, the formation of alumina-based coatings is more important. In this case, relatively inexpensive reactants may be used to obtain internal coatings of metallic pipes with very good abrasion and chemical resistance. However, it is very important to alter the violent nature of this chemical reaction by an addition of various additives which are responsible to make the alu-

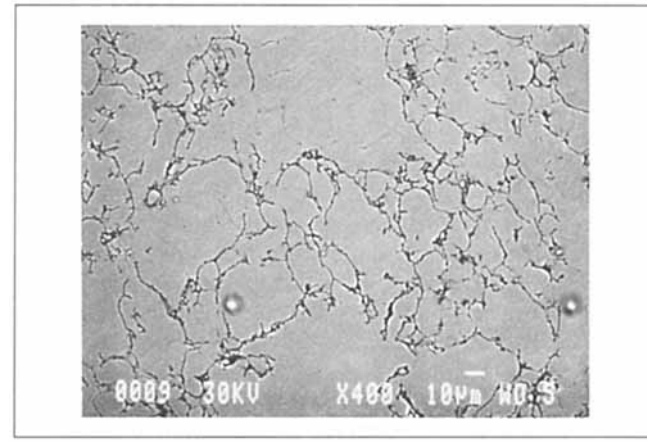

Figure 2. Microstructure of NiAl coating formed by SHS centrifugal densification technique.

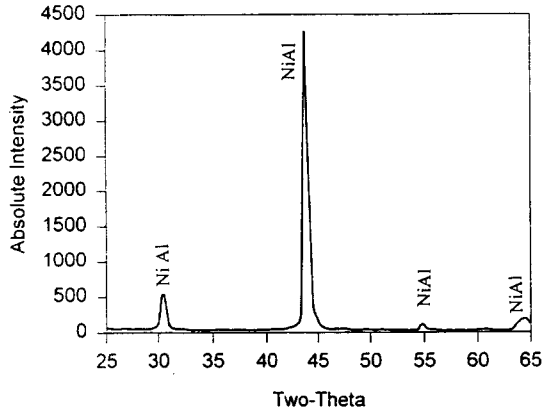

Figure 3. X-ray diffraction patterns of NiAl coating formed by SHS centrifugal technique, CuKα radiation source: $\lambda = 1.54050$ Å.

mina-based coating denser and free of cracks. The basic reaction occurring in this system can be represented as follow

$$Fe_2O_3 + yCr_2O_3 + 2(1+y)Al + \frac{4}{3}yC \rightarrow$$

$$2Fe + (1+y)Al_2O_3 + \frac{3}{2}yCr_3C_2$$

Due to the presence of other additives and their interaction with the primary reactants, the actual chemical reaction scheme is by far more complicated. The amount of chromium oxide used in this experimental study was varied between 10 and 30 wt. %. The other additives were added in the amount of 15–30 wt. % (10–18 $ZrSiO_4$ wt. %, 3–7 SiO_2 wt. %, 1–3 Na_2CrO_4 wt. %).

Each of these additives served a different purpose. Zircon, $ZrSiO_4$, was added in order to improve the high-temperature corrosion resistance of the coating. Silica and sodium chromate, on the other hand, improved the smoothness of internal surface, and led to a better separation of iron and alumina phases. Chromium oxide and carbon were added in order to improve properties of both the metallic and ceramic phases.

Cylindrical substrates were rotated with a speed between 1,000–2,000 rpm. The process is shown in Figure 1b. In this case the combustion front propagated both in axial and radial directions due to a local ignition at one end of the cylindrical substrate. When the rotating speed is not high enough, or the products cool too fast, the ceramic and iron phases are not separated completely (see Figure 4a). It can be seen that iron droplets are trapped within the ceramic layer. When higher rotating speeds were applied, a complete separation of both phases resulted (see Figure 4b). When coatings are used at high temperature, the transient zone between fully separated ceramic and metallic phases might be beneficial because it decreases the effect of their thermal expansion mismatch.

The analysis of the ceramic layer microstructure shows a significant difference along the radial direction which has not been observed by other researchers. The product was examined by a JSM-840 Scanning Electron Microscope. Semiquantitative EDS analysis was used to find the composition of key components. Phase identification was done using PHILIPS X-ray diffractometer.

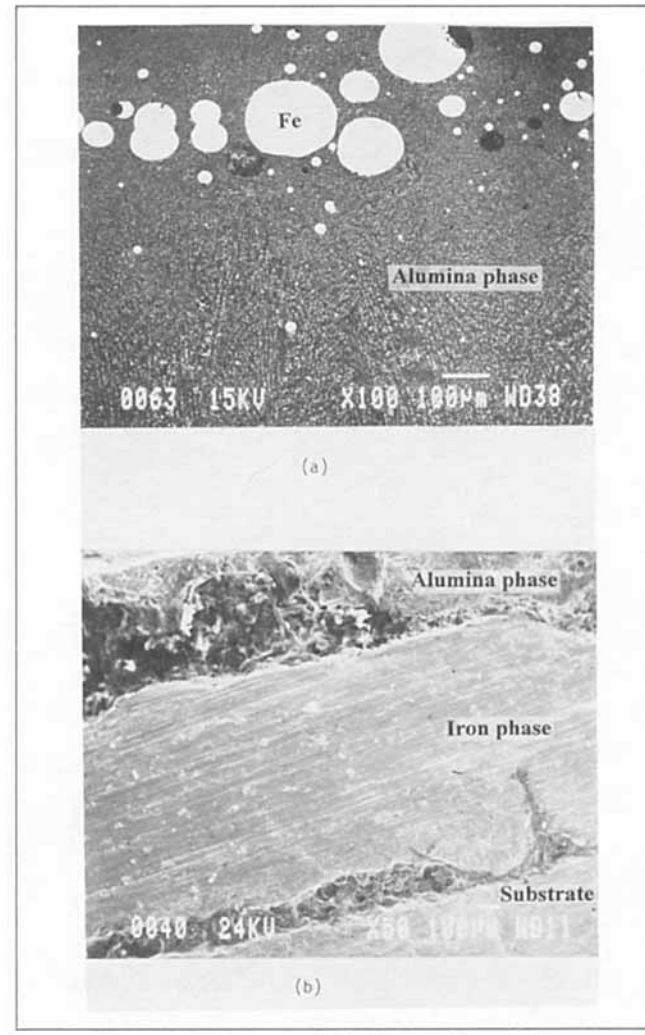

Figure 4. SEM of *in-situ* densified combustion products with centrifugal acceleration of: (a) 58 g; (b) 233 g.

Regular Al_2O_3 grains as shown in Figure 5 are found in the middle part of the ceramic layer and at the innermost surface. The grain sizes are largest at the innermost surface (Figure 5a) and decrease gradually toward the substrate surface (Figure 5b). Figure 6 represents the SEM backscattering photograph of the large ceramic grains at the innermost surface. These ceramic grains have a structure consisting of small alumina crystals. Heaver elements, iron and chromium, are dispersed along the boundary of these single alumina crystals. This identification was made using an EDS analyzer. X-ray and EDS analyses have indicated that the white dendrite structure shown in Figure 5b consists of zirconia (ZrO_2). Mullite has also been found at the interface between the zirconia and alumina phases. The radial distribution of grain sizes and composition of the key components are shown in Figures 7 through 9. The variation in grain sizes seems to be due to a significant temperature gradient in the radial direction with the highest temperature at the innermost surface.

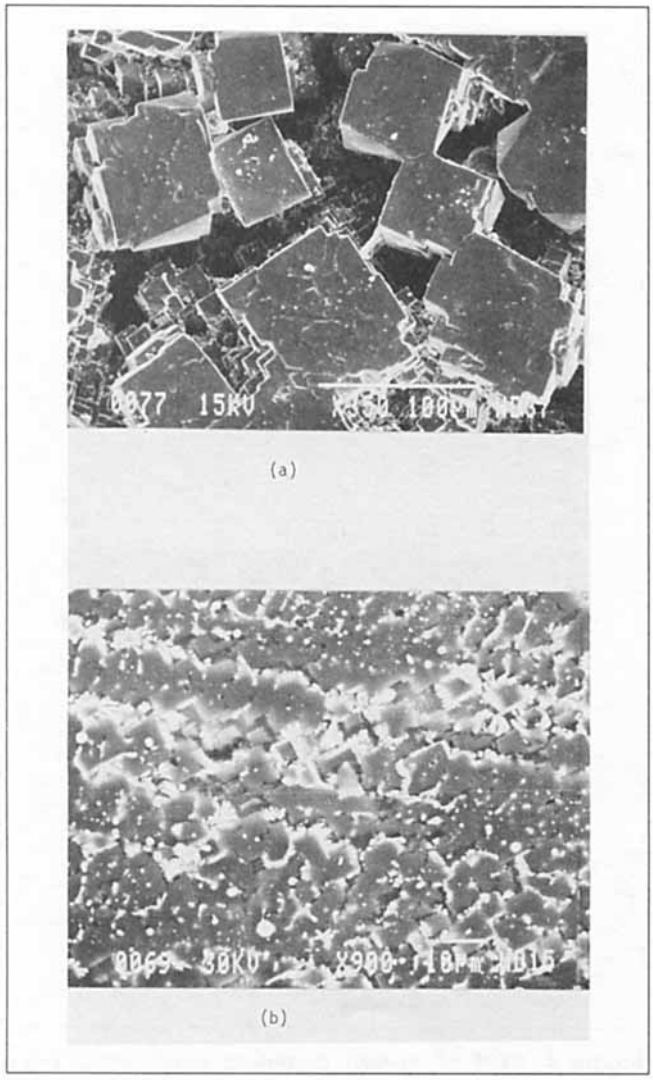

Figure 5. Microstructure of alumina-based layer formed in SHS densification process: (a) innermost surface; (b) middle part of the ceramic layer.

Cooling takes place mainly via conduction to the outer metallic substrate. As a result, the grains closer to the innermost surface are exposed to higher temperature for a longer time, and therefore their size is larger.

Measurement of kinetic parameters in Ni-Al system

Kinetic studies of the reaction between nickel and aluminum powders were done independently. Nickel and aluminum powders in a stoichiometric ratio, corresponding to the NiAl phase, were dry mixed for 4 h in a rotary mixer. Later, this mixture was diluted with the final product (NiAl) and was placed in the refractory boat (see Figure 10). The mixture of powders was then compacted to approximately 50% of the theoretical density (NiAl phase). Both an ignition coil and thermocouples were inserted into the reactant mixture. This boat was later placed inside the water cooled reactor. After three vacuum-inert gas (argon) purging operations, the reaction was initiated by passing an electrical current

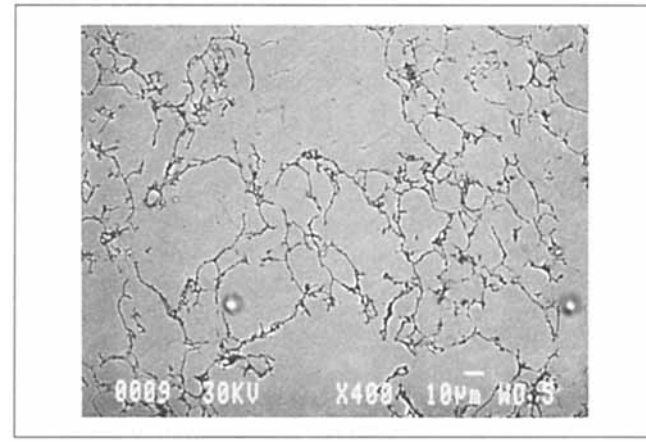

Figure 6. SEM backscattering of alumina crystals formed on the innermost surface.

through a molybdenum coil. Temperature profiles were measured by W (5% Rh)-W (25% Rh) thermocouples connected to the data acquisition system. The combustion front propagation was monitored with the Sony video camera system with a recording capability of thirty frames per second. Later, the velocity of the combustion front was calculated from both camera recording and responses of thermocouples placed at different positions in the sample. The experimental results are shown in Table 1. Both the activation energy and frequency factor were estimated using a nonisothermal technique described by Merzhanov (1981).

The relation between the combustion front velocity and the combustion temperature can be expressed

$$V_c^2 = \frac{kR_g T_c^2}{\rho(-\Delta H_r)E} Z_0 e^{-E/R_g T_c} \tag{1}$$

by plotting ln (V_c/T_c) vs. $1/T_c$ (see Figure 11); both activation energy E and frequency factor Z_0 were estimated and equal to 1.05×10^5 J/mol and 1.017×10^8 s^{-1}, respectively. The

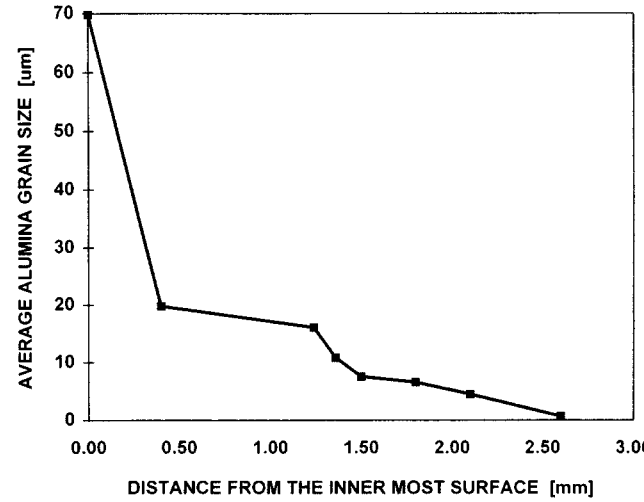

Figure 7. Radial distribution of average alumina grain sizes in the ceramic layer.

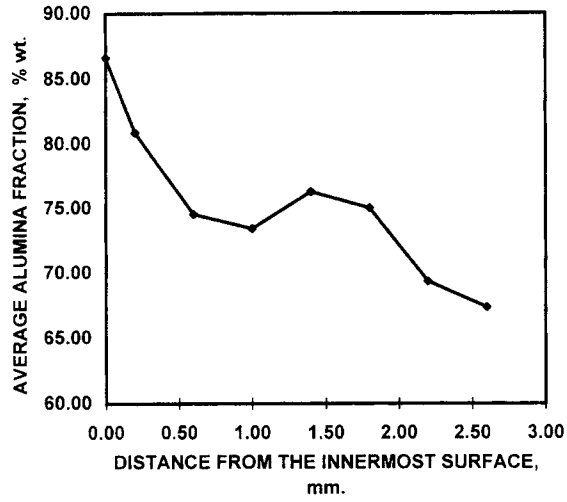

Figure 8. Radial distribution of alumina in the ceramic layer.

value of the activation energy is in a good agreement with the previously reported value by Itin and Naiborodenko (1989).

Modeling of SHS Centrifugal Densification

A mathematical model used in this analysis is based on the following assumption:

(1) Reactant powder mixture is initially well mixed and uniformly distributed inside a cylindrical pipe;

(2) A single phase product is formed during a gasless combustion process;

(3) A reactant mixture is uniformly ignited at the innermost surface and a combustion front propagates in a radial direction only;

(4) Shear and bulk viscosities of a combustion product can be expressed in a form of the power law fluid model (Stel'makh et al., 1991a, b; Buchatskii and Stolin, 1989);

(5) The viscosity of partially molten material is a function of liquid product fraction (Rahaman et al., 1987);

(6) Thermal conductivity of a densified material is calculated using both conduction and radiation mechanisms in a porous structure (Chlew and Glandt, 1983);

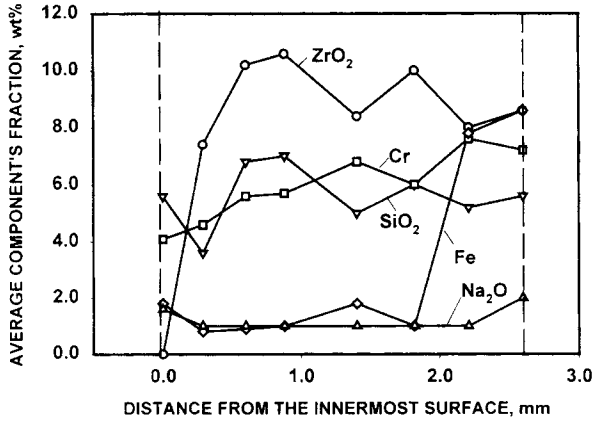

Figure 9. Radial distribution of other key components in the ceramic layer.

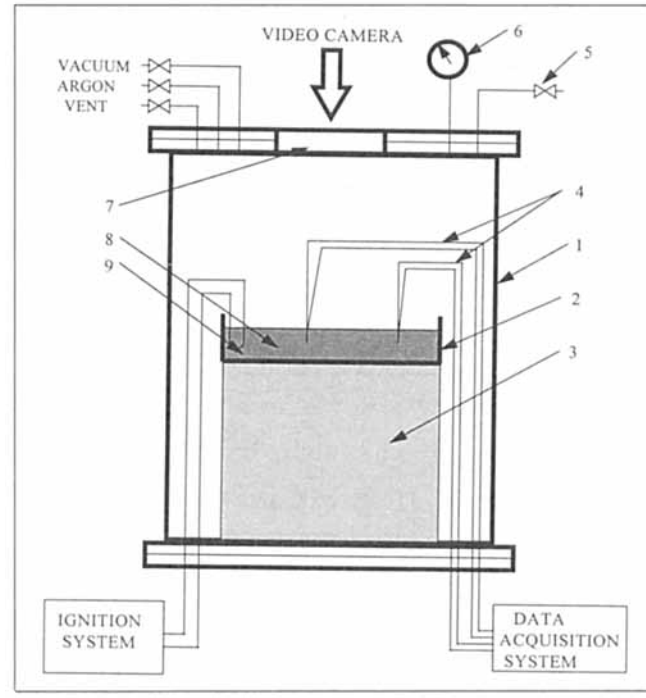

Figure 10. Experimental setup.

(1) Reactor; (2) refractory boat; (3) refractory support; (4) thermocouples; (5) safety relief valve; (6) pressure gauge; (7) glass window; (8) reacting mixture; (9) ignition coil.

(7) Heat capacity of the product can be expressed in a polynomial form.

A reactant mixture consisting of the stoichiometric mixture of Ni and Al powders is distributed inside a rotating refractory cylinder of an initial thickness $[R_s - r_i(0)]$ (see Figure 12). This mixture is uniformly ignited by a hot inert gas. Upon ignition, a combustion front propagates through the mixture in the outward direction. Due to very high temperatures generated in a combustion zone, the product of the exothermic reaction may be partially or completely molten and densification can be accomplished within seconds in a field of centrifugal forces.

A normal stress in the radial direction (stresses in axial and angular directions are assumed to be neglected due to a uniform propagation) can be expressed as follows

$$\tau_{rr} = -2\mu\frac{\partial v_r}{\partial r} - \left(\frac{2}{3}\mu - \chi\right)\left[\frac{1}{r}\frac{\partial}{\partial r}(rv_r)\right] \qquad (2)$$

Table 1. Velocity and Combustion Temperature in Ni-Al System

wt. % NiAl in React. Mix.	V_c ($m \cdot s^{-1}$)	Comb. Temp. T_c (K)	$1/T_c$ (K^{-1})	$\ln(V_c/T_c)$
0	0.035	1,905	0.000525	−10.9046
5	0.033	1,880	0.000532	−10.9503
10	0.031	1,865	0.000536	−11.0048
15	0.026	1,800	0.000556	−11.1452
20	0.024	1,760	0.000568	−11.2028
25	0.022	1,720	0.000581	−11.2668
30	0.020	1,700	0.000588	−11.3504
35	0.018	1,670	0.000599	−11.4380

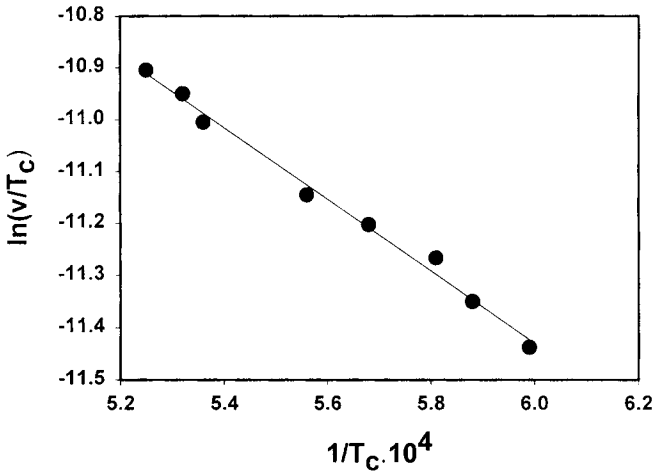

Figure 11. ln (V_c/T_c) vs. $1/T_c$ plot for Ni-Al system.

The centrifugal force (F) is expressed by

$$F = mr\bar{\omega}^2 \tag{3a}$$

$$F = \int_r 8\pi^3 N^2 L \rho r^2 dr \tag{3b}$$

Both shear, μ and bulk, χ viscosities ($kg \cdot m^{-1} \cdot s^{-1}$) are expressed in a form of the power law fluid model (Buchatskii and Stolin (1989).

Shear Viscosity:

$$\mu(\rho, T) = \mu_1(T)\mu_2(\rho) = \mu_0 \exp\left(\frac{U}{R_g T}\right)\gamma^n \tag{4}$$

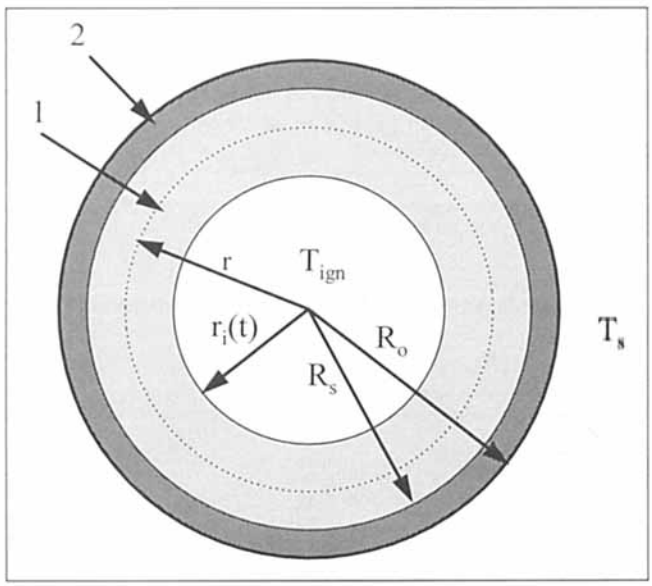

Figure 12. Cylindrical substrate and Ni-Al system.

Bulk Viscosity:

$$\chi(\rho, T) = \frac{4}{3}\mu(\rho, T)\frac{\gamma}{1-\gamma} = \frac{4}{3}\mu_0 \frac{\gamma^{n+1}}{1-\gamma}\exp\left(\frac{U}{R_g T}\right) \tag{5}$$

The centrifugal force per unit area acting on a densified material is equal to the opposite value of the radial stress.

$$\frac{1}{A}\int_r 8\pi^3 N^2 L \rho r^2 dr = 2\mu\frac{\partial v_r}{\partial r} - \left(\frac{2}{3}\mu - \chi\right)\left(\frac{1}{r}\frac{\partial}{\partial r} r v_r\right) \tag{6}$$

The continuity equation in the cylindrical coordinates is as follows

$$\frac{\partial \rho}{\partial t} + \frac{1}{r}\frac{\partial}{\partial r}(\rho r v_r) = 0 \tag{7}$$

The reaction between nickel and aluminum is self-sustaining when ignited. The material and energy balance equations read

$$\frac{dX}{dt} = Z_0 e^{-E/R_g T}(1 - X) \tag{8}$$

$$\rho\frac{\partial H}{\partial t} = A_1 + B_1 + C_1 \tag{9}$$

where

$$A_1 = \frac{1}{r}\frac{\partial}{\partial r}\left(kr\frac{\partial T}{\partial r}\right) \tag{10a}$$

$$B_1 = 2\mu\left[\left(\frac{\partial v_r}{\partial r}\right)^2 + \left(\frac{v_r}{r}\right)^2\right] \tag{10b}$$

$$C_1 = -\Delta H_r \frac{dX}{dt} + v_r \rho T C_p \tag{10c}$$

In order to make this moving boundary value problem more suitable for numerical calculations, the Lagrange coordinate (kg) system was used

$$q(r, t) = \int_r 2\pi\rho r dr \tag{11}$$

The governing equations after transformation read

$$\frac{4\pi^2 N^2}{A}\int_0^q r dq = 4\pi L\mu\frac{\partial(\rho r v_r)}{\partial q} - \left(\frac{2}{3}\mu - \chi\right)\frac{2\pi L}{r}\frac{\partial(\rho_r^2 v_r)}{\partial q} \tag{12}$$

$$\frac{\partial \rho}{\partial t} + \frac{2\pi L}{r}\frac{\partial}{\partial q}(\rho^2 r^2 v_r) = 0 \tag{13}$$

$$\rho\frac{\partial H}{\partial t} = A_2 + B_2 + C_2 \tag{14}$$

where

$$A_2 = \frac{4\pi^2 L^2}{r}\frac{\partial}{\partial q}\left[\rho k r^2 \frac{\partial (T\rho r)}{\partial q}\right] \tag{15a}$$

$$B_2 = 2\mu\left[\left(2\pi L \frac{\partial(\rho r v_r)}{\partial q}\right)^2 + \left(\frac{v_r}{r}\right)^2\right] \tag{15b}$$

$$C_2 = -\Delta H_r \frac{\partial X}{\partial t} + v_r \rho T C_p \tag{15c}$$

The initial and boundary conditions are

$$t \le 0;\ 0 \le q \le q_{\max}:\ v_r = 0,\ X = 0,\ T = T_{\text{in}};\ \gamma = \gamma_{\text{in}} \tag{16}$$

$$t > 0;\ q = 0;\ 2\pi k_1 L \rho r \left.\frac{\partial T}{\partial q}\right|_{r = r_i(t)} = h_i[T_{ign} - T_i(t)] \tag{17}$$

$$q = q_{\max}:\ 2\pi L \rho r k_1 \left.\frac{\partial T}{\partial q}\right|_{q_{\max}} = k_2 \left.\frac{\partial T}{\partial r}\right|_{r = R_s^+};\ \frac{\partial v_r}{\partial q} = 0;\ \frac{\partial r}{\partial q} = 0 \tag{18}$$

The enthalpy H ($J \cdot kg^{-1}$) has been calculated as follows (Voller, 1987; Gatica et al., 1995)

$$T < T_m \qquad H = C_P T \tag{19a}$$

$$T = T_m \qquad H = C_p T + \Delta H_m f \tag{19b}$$

$$T > T_m \qquad H = C_{p,liq} T \tag{19c}$$

The additional boundary condition for the heat transfer in a cylindrical substrate is

$$r = R_0;\quad -k_2 \frac{\partial T}{\partial r} = h_0[T(R_0, t) - T_s] \tag{20}$$

Equations 8 through 14 were solved numerically using a finite difference implicit method. Both the number of radial grid points and the integration time were varied in these simulations in order to obtain results with a relative error less than 5%. Finally, the Richardson extrapolation was also applied. Typically, 200–400 grid points and time step $10^{-8} - 10^{-6}$ s were needed to satisfy the accuracy.

Other parameters used in these numerical simulations are presented in Table 2. Typical dynamic profiles at the middle of the densified material are shown in Figure 13. When the combustion front reaches this point, the local temperature suddenly increases and reaches the melting point of nickel aluminide, 1,911 K (Figure 13b). The product of this exothermic reaction (nickel aluminide) partially melts in and behind the combustion front. Fraction of the molten product as a function of time in the middle section of the densified material is shown in the Figure 13c. Figure 13a shows the dynamics of the densification at the same position. The densification process strongly depends on centrifugal acceleration. Typical temperature and density profiles for two different rotational speeds are shown in Figures 14 and 15. At the lower rotational speed (~ 1,500 rpm), the combustion front propagates toward a substrate surface with almost constant velocity. Each temperature profile is plotted at the constant time increment of 0.015 s. It can be clearly seen from Figure 14a that the position of the innermost surface does not move significantly. Therefore, the product does not densify (see Figure 14b). At higher rotating speed, the densification process

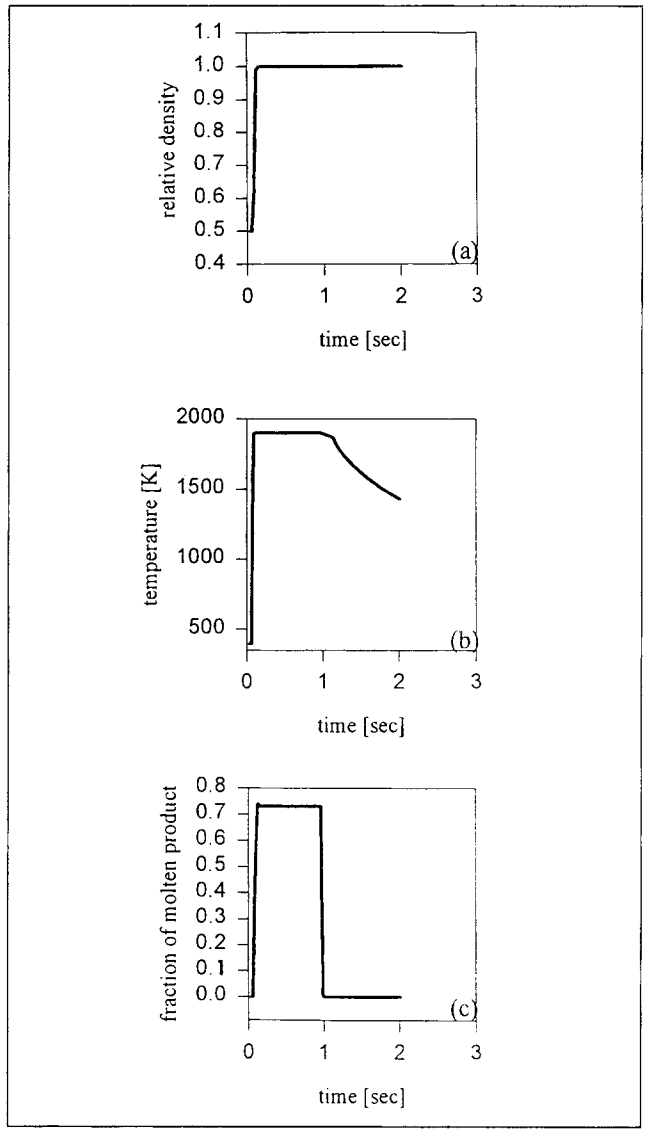

Figure 13. Dynamic profiles of the middle of the densified material.

(a) Relative density; (b) temperature; (c) fraction of a molten product (see Table 2).

Table 2. Parameters Used in Numerical Simulations

Symbols	Values	Reference
n	1	Buchatskii and Stolin (1989)
ΔH_m (kJ/mol)	40.03	Itin and Naiborodenko (1989)
ΔH_r (kJ/mol)	117.74	Itin and Naiborodenko (1989)
ρ_s (kg/m^3)	5250	this work
E (J/mol)	1.05×10^5	this work
Z_0	1.017×10^8	this work

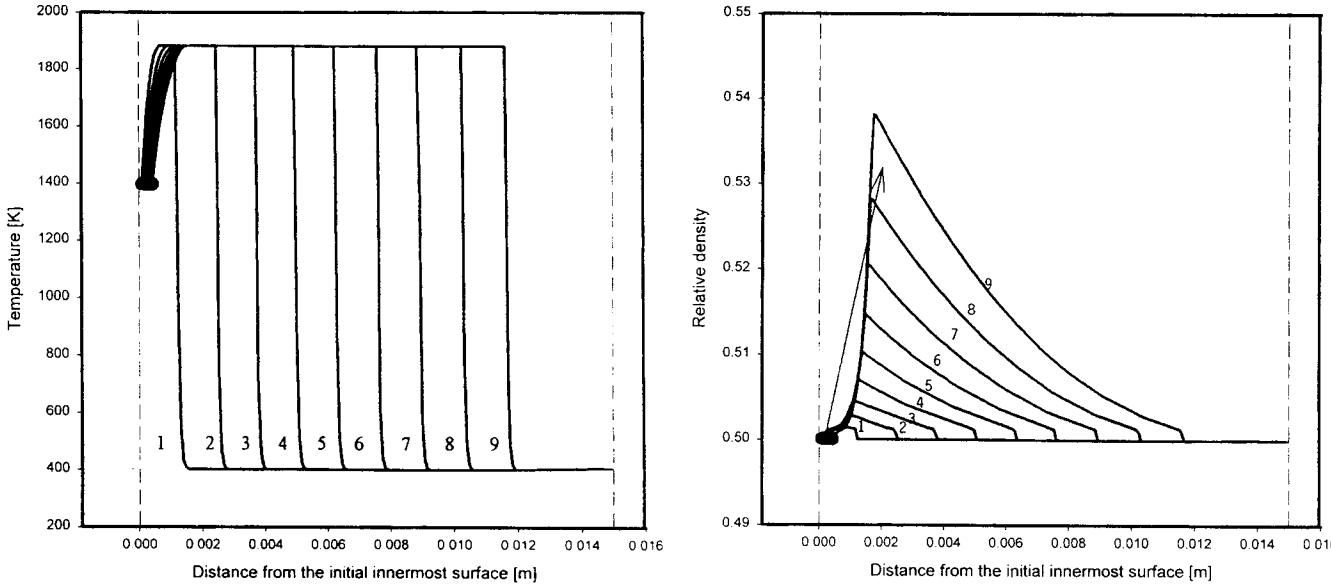

Figure 14. Temperature and densification of NiAl during SHS centrifugal densification of NiAl.

Rotational speed, 1,500 rpm (other parameters in Table 2); 1–0.015 s, other profiles with time increment of 0.015 s.

is more dominant and it is completed for rotating speed higher than 3,000 rpm (see Figures 15a and 15b).

Conclusions

Simultaneous combustion synthesis and densification is a highly energy efficient method. *In-situ* densification in the field of centrifugal forces can result in a formation of dense intermetallic or alumina based coatings.

An addition of silica, zircon, and chromium oxide significantly reduces the porosity of alumina coatings and increases both internal surface smoothness and hardness. It was found that both the composition and grain sizes of ceramic layer vary significantly in the radial direction.

Activation energy E ($J \cdot mol^{-1}$) and frequency factor Z_0 (s^{-1}) for Ni-Al reacting system were evaluated using non-isothermal technique and found equal to 1.05×10^5 J/mol and 1.017×10^8 s^{-1}, respectively.

The presented mathematical model allows to perform a qualitative analysis of simultaneous combustion synthesis of a single-phase product and its densification in the field of centrifugal forces. However, due to the lack of reliable data on transport properties at elevated temperature, further research is needed to perform a quantitative analysis which could be used to scale up the SHS-densification process.

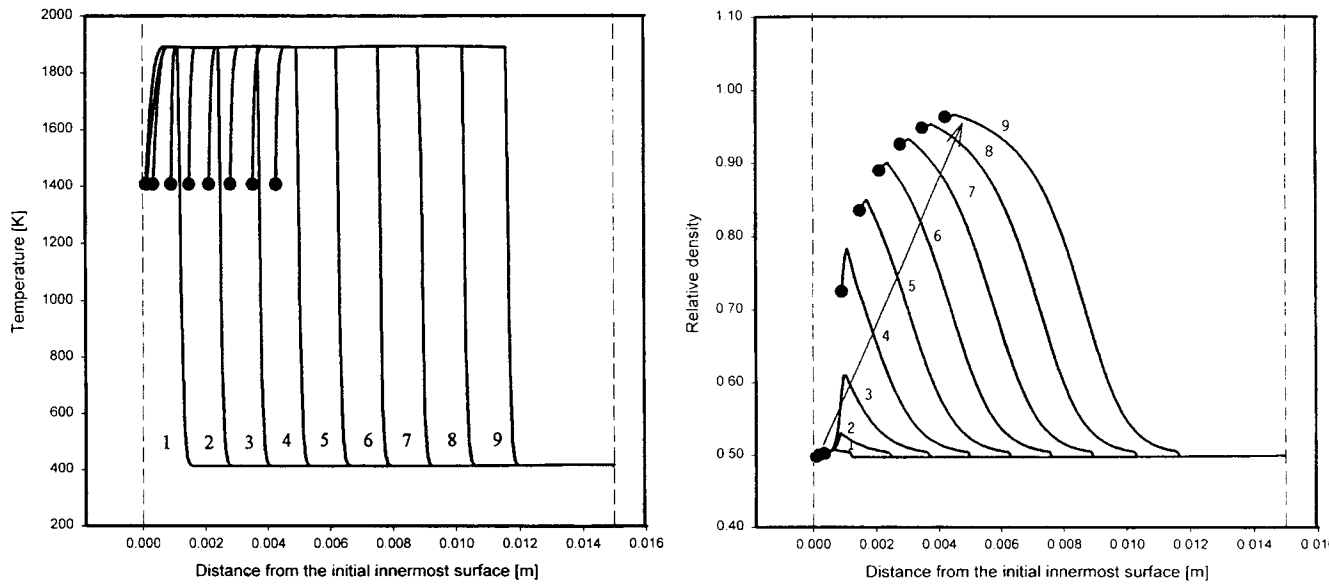

Figure 15. Temperature and density profiles during SHS centrifugal densification of NiAl.

Rotational speed, 3,500 rpm (other parameters in Table 2); 1–0.015 s, other profiles with time increment of 0.015 s.

Acknowledgment

The authors of this article gratefully acknowledge the financial support from the National Science Foundation (grant No. CTS-9309561).

Notation

C_p = heat capacity, $J \cdot K^{-1} \cdot kg^{-1}$
f = molten fraction of molten product
h_0 = heat-transfer coefficient, $W \cdot m^{-2} \cdot s^{-1}$
ΔH_m = heat of melting, $J \cdot kg^{-1}$
ΔH_r = heat of reaction, $J \cdot kg^{-1}$
k = coefficient of thermal conductivity, $W \cdot m^{-1} \cdot s^{-1}$
L = length of a cylindrical substrate, m
m = mass, kg
N = rotation speed (revolution per second)
r = radial coordinate, m
R_g = universal gas constant, $8.314\ J \cdot mol^{-1} \cdot K^{-1}$
R = radius, m
t = time, s
T = temperature, K
U = activation energy (viscosity), $J \cdot mol^{-1}$
v_r = velocity, $m \cdot s^{-1}$
X = conversion
γ = relative density
ρ = density, $kg \cdot m^{-3}$
τ_{rr} = shear stress, $N \cdot m^{-2}$
ω = angular speed, s^{-1}

Subscripts and superscripts

1 = product
2 = substrate
o = outer
c = combustion
i = inner
ign = ignition state
in = initial state
m = melting

Literature Cited

Buchatskii, L. M., and A. M. Stolin, "Determining the Rheological Properties of Compressible Powder Materials in the High-Temperature Range, *Inz. Fiz. Zh.*, **57**(4), 645 (1989).

Chlew, Y. C., and E. D. Glandt, "Simultaneous Conduction and Radiation in Porous and Composite Materials: Effective Thermal Conductivity," *Ind. Eng. Chem. Fund.*, **22**(3), 276 (1983).

DeAngelis, T. P., and D. S. Weiss, *Advance Ceramics via SHS, Combustion and Plasma Synthesis of High-Temperature Materials*, Z. A. Munir and J. B. Holt, eds., VCH Publishers, New York, p. 144 (1990).

Frankhauser, W. L., K. W. Brendley, M. C. Kieszek, and S. T. Sullivan, *Gasless Combustion Synthesis of Refractory Compounds*, Noyes Publications, Park Ridge, NJ (1985).

Gatica, J. E., P. A. Dimitriou, J. A. Puszynski, and V. Hlavacek, "Melting Effects of Reaction Front Propagation in Gasless Combustion," *Int. J. of Self-Propagating High-Temperature Synthesis*, **4**(2), 123 (1995).

Grebe, H. A., A. Advani, N. N. Thadhani, and T. Kottke, "Combustion Synthesis and Subsequent Explosive Densification of Titanium Carbide Ceramics," *Metall. Trans. A*, **23A**, 2365 (1992).

Itin, V. I., and Y. S. Naiborodenko, *High Temperature Synthesis of Intermetallic Compounds*, Tomsk Publications, Tomsk, Russia (1989).

Luss, D., "Reaction Engineering of Advanced Materials," *Chem. Eng. Sci.*, **45**(8), 1979 (1990).

McCauley, J. W., "An Historical and Technical Perspective on SHS," *Ceram. Eng. Sci. Proc.*, **11**(9-10) (1990).

Merzhanov, A. G., "SHS Process: Combustion Theory and Practice," *Archivum Combustionis*, **1**, 23 (1981).

Merzhanov, A. G., *Self-Propagating High Temperature Synthesis: Twenty Years of Search and Findings, Combustion and Plasma Synthesis of High Temperature Materials*, Z. A. Munir and J. B. Holt, eds., VCH Publishers, New York, p. 1 (1990).

Merzhanov, A. G., and V. I. Yukhvid, "The Self-Propagating High-Temperature Synthesis in the Field of Centrifugal Forces," *Proc. U.S.-Japanese Workshop on Combustion Synthesis*, Kaieda and Holt, eds., NRIM, Tokyo, Japan, p. 1 (1989).

Munir, Z. A., and U. Anselmi-Tamburini, "Self-Propagating Exothermic Reactions: The Synthesis of High Temperature Materials by Combustion," *Mater. Sci. Rep.*, **3**, 277 (1989).

Odawara, O., "Long Ceramic-Lined Pipes Produced by a Centrifugal Process," *J. Amer. Ceram. Soc.*, **73**(3), (1990).

Puszynski, J. A., D. S. Kattamuri, B. Stefansson, and S. Jagarlamudi, "Simultaneous Combustion Synthesis and Densification with Product Separation," *Adv. Powder Metall. and Particulate Materials*, **2**(7), 187 (1995).

Rahaman, M. N., L. C. De Jongke, G. W. Scherer, and R. J. Brook, "Creep Densification During Sintering of Glass Powder Compacts," *J. Amer. Ceram. Soc.*, **70**, 766 (1987).

Stel'makh, L. S., A. M. Stolin, and B. M. Khusid, "Nonisothermal Rheology during SHS-Densification of Powder Materials," *Inz. Fiz. Zh.*, **61**(1), 33 (1991).

Stel'makh, L. S., A. M. Stolin, and B. M. Khusid, "Extrusion Rheodynamics for a Viscous Compressible Material," *Inz. Fiz. Zh.*, **61**(2), 268 (1991).

Smolyakov, V. K., "Macrostructural Changes during Combustion of Gasless Mixtures in Molds," *Fizika Goreniya i Vzryva*, **26**(2), 73 (1988).

Varma, A., and J. P. Lebrat, "Combustion Synthesis of Advanced Materials," *Chem. Eng. Sci.*, **47**, 2179 (1992).

Voller, V. R., "An Implicit Enthalpy Solution for Phase Change Problems: With Application to a Binary Alloy Solidification," *Appl. Math. Modeling*, **11**, 110 (1987).

Yin, S., M. Liu, C. Yao, and Z. Guo, "Feldspar Additive in Ceramic Composite Pipes Made by a Centrifugal SHS Process," *Int. J. Self-Propagating High-Temperature Synthesis*, **2**(1), 69 (1993).

Manuscript received Oct. 28, 1996, and revision received June 30, 1997.